Eleventh International Conference on Computational Fluid Dynamics (ICCFD11), Maui, Hawaii, July 11-15, 2022 **ICCFD11-2022-0801**

Fluid-structure interaction with multi-body collision: application to collective fish swimming in an impermeable or porous enclosure

M. Bergmann*
Corresponding author: michel.bergmann@inria.fr

* Memphis Team, INRIA, F-33400 Talence, France
Univ. Bordeaux, IMB, UMR 5251, F-33400 Talence, France
CNRS, IMB, UMR 5251, F-33400 Talence, France

Abstract: This work is dedicated to the numerical modeling of collective swimming in an enclosure. Collective swimming involves several complex physical phenomena such as fluid-structure interactions and possible contacts and collisions between fishes. Collective swimming in an enclosure necessarily leads to some collisions between fishes and the enclosure boundary. We present here the whole numerical framework allowing to perform parallel numerical simulations of self propelled locomotion with collisions. Numerical simulations show that different swimming behaviors could be observed for porous and impermeable enclosures.

Keywords: Computational Fluid Dynamics, bio-inspired swimming, collision modeling.

1 Introduction

The numerical modeling of fish like swimming has been largely studied over the last two decades [1, 2, 3, 4]. These numerical simulations can compliment some experimental observations [5, 6, 7] with quantitative results, for instance by computing the power spent by the fish. The detailed comprehension of the involved phenomena may also help engineers to conceive new generations of AUVs [8, 9] with enhanced efficiency and maneuverability compared to those observed in other classical locomotion modes based on propellers.

Fish schooling is another way to save energy for the locomotion [10, 11, 12]. However, fish schooling has been hardy considered numerically in the literature [2], the main difficult point being probably the modeling of possible contacts and collisions between swimmers. Indeed, extra modeling efforts have to be done, since, by definition, contacts occurs when no fluid remains near the contact point, and thus are not included in the fluid governing model like the Navier-Stokes equations. This extra contact modeling, called lubrication, is usually based on theoretical Stokes flow models for simple geometries like spheres and plane walls [13, 14, 15]. Collision models with possible rebounds are usually based on soft-sphere collision [16]. In the past, we have developed local lubrication models allowing to consider collisions between spherical and ellipsoidal geometries [17, 18]. The goal is here to extend these models for collisions between obstacles with arbitrary geometries. More precisely, we will consider small fish schools, typically limited to three swimmers, swimming in a circular enclosure. The contacts will thus be between fishes, and between fish and the enclosure boundary. We will consider three-dimensional configurations with porous or impermeable enclosures.

After having introduced the general problem under consideration, including the flow configuration and the governing equations in §2, we will present preliminary numerical results for the swimming of three fishes in porous and impermeable enclosure in §3. We finally present some conclusions and perspectives in §4.

2 Problem Statement

In this paper, we consider the multi-body interactions of self propelled swimmers in an enclosure, where the general configuration is described in §2.1. We will introduce the complete model used to solve the fluid-structure interaction, including the general model for the fluid in §2.2, the fictitious approach to take into account the bodies in §2.3, the interface modeling in §2.4 and the fish geometry and swimming law in §2.5. The model used to take into account lubrication and collision forces and torques is then introduced in §2.6. The numerical methods used the solve the whole model are then briefly described in §2.7.

2.1 Flow configuration

A sketch of the flow configuration is given in Figure 1. We considered N_S self propelled bodies, in domains $\{\Omega_S^{(i)}\}_{i=1}^{N_S}$, swimming in a domain Ω_F^{int} filled with a viscous and incompressible fluid (water). The domain Ω_F^{int} is inside an enclosure represented by the domain Ω_E. The domain Ω_F^{ext}, outside the enclosure, is filled with the same fluid as in the domain Ω_F^{int}. The whole domain under consideration is $\Omega = \Omega_F^{int} \cup \Omega_E \cup \Omega_F^{ext} \cup_{i=1}^{N} \Omega_S^{(i)}$. The external boundary is defined by Γ_{ext}. Other interfaces are also introduced. The interface between the external domain Ω_F^{ext} and the enclosure Ω_E is Γ_E^{ext}, the interface between the internal domain Ω_F^{int} and the enclosure Ω_E is Γ_E^{int}, and the interface between the internal domain Ω_F^{int} and the i^{th} swimmers $\Omega_S^{(i)}$ is $\Gamma_S^{(i)}$. While the swimmers are impermeable, the enclosure can be impermeable or porous. The generation of an unsteady flow in domains Ω_E and Ω_F^{ext} is obtained with a porous enclosure. In what follows, we consider a three-dimensional configuration. We imposed a small distance between the bottom wall and the enclosure, δ_{bottom}, and between the top boundary and the enclosure, δ_{top}. The fluid domains Ω_F^{int} and Ω_F^{ext} are thus connected to form a single domain Ω_F, and we have $\Omega = \Omega_F \cup \Omega_E \cup_{i=1}^{N} \Omega_S^{(i)}$

The size of the three-dimensional domain is $L_X \times L_Y \times L_Z$. The general flow configuration is presented in Figure 1.

The domains and interfaces introduced before depend on time, and are mathematically defined by level-set scalar functions [19, 20]. Here, the i^{th} swimmer in domain $\Omega_S^{(i)}$ is arbitrarily defined by $\psi_S^{(i)} > 0$ inside the swimmer, by $\psi_S^{(i)} = 0$ on its interface $\Gamma_S^{(i)}$ and by $\psi_S^{(i)} < 0$ elsewhere. The enclosure is also arbitrarily defined by a level-set $\psi_E > 0$ inside the enclosure, $\psi_E = 0$ on its interface, and $\psi_E < 0$ elsewhere.

Finally the water domain Ω_F is defined by $\psi_F < 0$, where $\psi_F = \max(\psi_E, \max_i \psi_S^{(i)})$. We thus have $\psi_F = 0$ on all interfaces, and $\psi_F > 0$ inside the swimmers and the enclosure.

2.2 Modeling and governing equations

The velocity field is $\boldsymbol{u} = (u,\, v,\, w) \in \mathbb{R}^3$, where u, v and w denote the velocity components in the x, y and z directions respectively, and $p \in \mathbb{R}$ is the pressure field. The viscous part of the stress tensor is $D(\boldsymbol{u}) = \dfrac{\boldsymbol{\nabla u} + \boldsymbol{\nabla}^T \boldsymbol{u}}{2}$. The incompressible Navier-Stokes equations in domain Ω_F are:

$$\frac{\partial \boldsymbol{u}}{\partial t} + (\boldsymbol{u} \cdot \boldsymbol{\nabla})\boldsymbol{u} = -\frac{1}{\rho}\boldsymbol{\nabla} p + \frac{1}{\rho}\boldsymbol{\nabla} \cdot 2\mu D(\boldsymbol{u}) + \boldsymbol{g} \text{ in } \Omega_F, \tag{1}$$

$$\boldsymbol{\nabla} \cdot \boldsymbol{u} = 0 \text{ in } \Omega_F, \tag{2}$$

with initial conditions $\boldsymbol{u}(\boldsymbol{x},\, t = 0) = \boldsymbol{u}_0$ and $p(\boldsymbol{x},\, t = 0) = p_0$, boundary conditions on the external boundary for both velocity $\boldsymbol{u(x,\, t)}$ and pressure $p(\boldsymbol{x},\, t)$ on $\boldsymbol{x} \in \Gamma^{ext}$, and boundary conditions on the structure boundaries (swimmers and enclosure).

On the fluid-swimmer interface, we have:

$$\boldsymbol{u}(\boldsymbol{x},\, t) = \widehat{\boldsymbol{u}}_S^{(i)}(\boldsymbol{x},\, t) \text{ on } \Gamma_S^{(i)}, \tag{3}$$

where the velocity $\widehat{\boldsymbol{u}}_S^{(i)}(\boldsymbol{x},\, t)$ will be described later on. On the fluid-enclosure interface we impose

$$\boldsymbol{u}(\boldsymbol{x},\, t) = \boldsymbol{0} \text{ on } \Gamma_E. \tag{4}$$

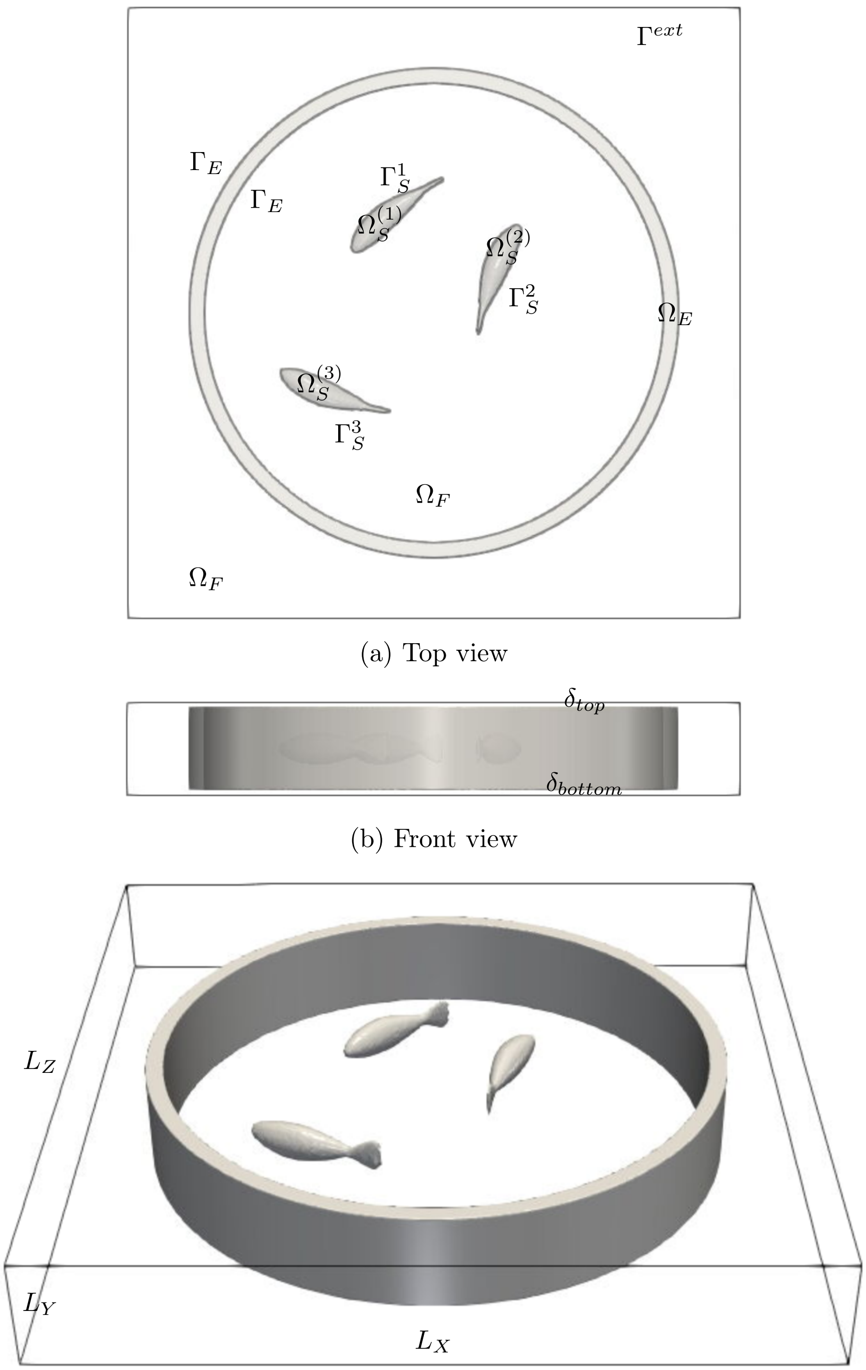

(a) Top view

(b) Front view

(c) Top/Front view

Figure 1: Sketch of the flow configuration.

2.3 Fictitious domain approach: the Volume Penalization method

One of the main difficulties in the numerical resolution of the Navier-Stokes equations (1) and (2) with internal boundary conditions (3) and (4) is that the interfaces $\Gamma_S^{(i)}$ and the domain Ω_F are time dependent. Several approaches to take into account unsteady interface condition (3) can be envisioned.

This first class of methods is based on body-fitted grids. In these methods, degrees of freedom are put on the interfaces, and it is thus possible to impose directly the interface condition (3). Mesh deformation can be handle with arbitrary Lagrangian-Eulerian (ALE) method. These methods are accurate, but require mesh adaptation and a mesh partitioner for parallel computations.

A second class of methods, adopted in this study, is based on fictitious domain approaches. In these approaches, the interfaces and associated domains do not covered the same mesh nodes at each time step: the interface can cross a fixed mesh, and no interface markers are thus required. Simple meshes like Cartesian ones can be used. The drawback is that the accuracy at interfaces can be degraded, and an extra work has to be performed to acurately model the interfaces.

In fictitious approaches, an extra term is added in the momentum equations (1) to take into account the condition (3) and (4). The condition on the fluid-structure interface is modeled with an extra term $\boldsymbol{s}$.

The system (1)-(4) is thus recasted in a system written in the whole domain Ω:

$$\frac{\partial \boldsymbol{u}}{\partial t} + (\boldsymbol{u} \cdot \boldsymbol{\nabla})\boldsymbol{u} = -\frac{1}{\rho}\boldsymbol{\nabla} p + \frac{1}{\rho}\boldsymbol{\nabla} \cdot 2\mu D(\boldsymbol{u}) + \boldsymbol{s} \quad \text{in } \Omega, \tag{5}$$

$$\boldsymbol{\nabla} \cdot \boldsymbol{u} = 0 \quad \text{in } \Omega, \tag{6}$$

Among the most popular fictitious approches are the Immersed Boundary Methods (IBM) originally introduced in [21] and later on used in several studies [22, 23, 24], and the Volume Penalization (VP) method introduced in [25] and used for instance in biolocomotion problems [2, 3, 4]. Another approach combining IBM and VP has been developed in [26]. In this study, the VP method is used with

$$\boldsymbol{s} = \sum_{i=1}^{N_S} \lambda_S^{(i)} \chi_S^{(i)} (\widehat{\boldsymbol{u}}_S^{(i)} - \boldsymbol{u}) - \lambda_E \chi_E \boldsymbol{u}. \tag{7}$$

Here, $\chi_S^{(i)} = H(\psi_S^{(i)})$, *i.e.* $\chi_S^{(i)} = 1$ inside $i^{th}$the swimmer , and $\chi_S^{(i)} = 0$ outside. Similarly, $\chi_E = H(\psi_E)$. As perviously defined in (3), $\widehat{\boldsymbol{u}}_S^{(i)}$ is the velocity inside the i^{th} swimmer. Parameters $\lambda_S^{(i)}$ and λ_E are linked to the porosity of the bodies. Since we will consider impermeable swimmers, we chose a large value for $\lambda_S^{(i)}$, and we impose $\lambda_S^{(i)} = 10^8$. The enclosure can be either porous and impermeable, and we thus chose $\lambda_E = 10^8$ for impermeable enclosure, and $\lambda_E = 10$ for porous enclosure. The computation of $\widehat{\boldsymbol{u}}_S^{(i)}$ will be detailed in §2.5.

2.4 Interface tracking

All bodies (swimmers and enclosure) are defined with markers on their interfaces. The surface of the i^{th} swimmer $\Gamma_S^{(i)}$ is approximated by a mesh (*i.e.* with markers), and a Lagrangian transport is used for any mesh point $\boldsymbol{x}_h^{(i)}$:

$$\frac{\mathrm{d}\boldsymbol{x}_h^{(i)}}{\mathrm{d}t} = \widehat{\boldsymbol{u}}_h^{(i)}, \tag{8}$$

where $\widehat{\boldsymbol{u}}_h^{(i)}$ is the restriction of $\widehat{\boldsymbol{u}}_S^{(i)}$ on the swimmer mesh boundary.

The signed distance function is recovered computing the minimal distance to the interface:

$$\psi_s(\boldsymbol{x}) = \min_{\boldsymbol{y} \in \Gamma_s} \|\boldsymbol{x} - \boldsymbol{y}\|_2 S(\boldsymbol{x}). \tag{9}$$

where $S(\boldsymbol{x})$ denotes a sign function applied on a point $\boldsymbol{x}$, with $S(\boldsymbol{x}) > 0$ inside the body, and $S(\boldsymbol{x}) < 0$ outside. This sign function can be computed with simple geometric arguments, from the outward normal to the body.

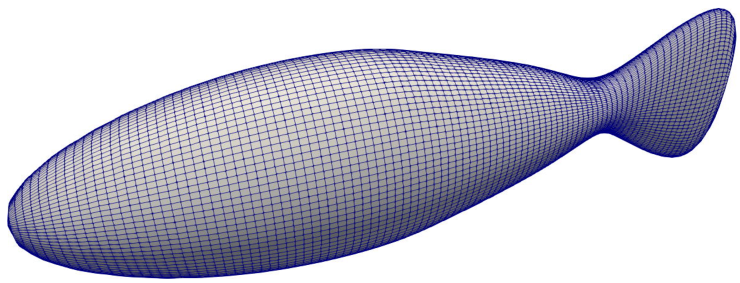

Figure 2: Geometry of the swimmers.

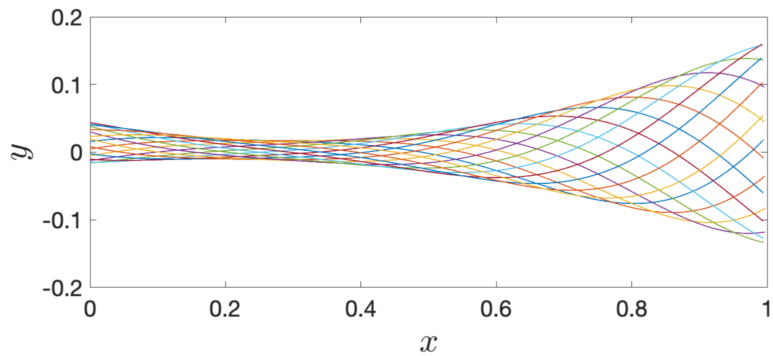

Figure 3: Swimming law applied to the midline (backbone).

2.5 Swimmers model

The geometry of the undeformed swimmers is inspired by a simplified fish body, see Figure 2. The swimming law is defined by a deformation of the swimmer midline, also called the backbone.

We consider a backbone deformation in the plan $(0, x, y)$ of swimmer in Figure 2, where point O is at the front head of the swimmer and x positive to the right. We consider also that the midline for the steady body is $0 \leq x \leq \ell$, $y = 0$, where the length of the swimmer is ℓ.

Many fishes impose a periodic swimming law [5]:

$$y(x,\, t) = a(x) \sin(k\, x - \omega\, t), \tag{10}$$

where $k = 2\pi/\lambda$ is the wavenumber, corresponding to wavelength λ, ω is the circular frequency of oscillations, and where $a(x) = A/2(c_0 + c_1 x + c_2 x^2)$ is the envelop. Different swimming laws can be found in [27] and [28]. To mimic a thunniform like swimming, we impose $A = 1.2$, $c_0 = 0.02$, $c_1 = -0.12$ and $c_2 = 0.2$ for a unit length fish with $0 \leq x \leq 1$. Several midline deformations are presented in Figure 3 over one stroke.

The body velocity of the i^{th} swimmer is

$$\widehat{\boldsymbol{u}}_S^{(i)}(\boldsymbol{x},\, t) = \overline{\boldsymbol{u}}_i(\boldsymbol{x},\, t) + \boldsymbol{u}_i^{\theta}(\boldsymbol{x},\, t) + \widetilde{\boldsymbol{u}}_i(\boldsymbol{x},\, t) \quad \forall \boldsymbol{x} \in \Omega_s, \tag{11}$$

where $\overline{\boldsymbol{u}}(\boldsymbol{x},\, t)$ is the linear velocity, $\boldsymbol{u}^{\theta}(\boldsymbol{x},\, t)$ is the angular velocity and $\widetilde{\boldsymbol{u}}(\boldsymbol{x},\, t)$ is the deformation velocity. While the deformation $\widetilde{\boldsymbol{u}}(\boldsymbol{x},\, t)$ has to be imposed by swimmer muscles, the linear and angular velocities are the results of the loads generated by the fluid on the body, and are computed from the Newton's laws. In this study, we consider the fish as an Euler-Bernouli beam, *i.e.* each orthogonal section to the undeformed midline remains orthogonal to the midline during the deformation. In order to remove extra forces and torques generated by the deformation, a Procrustes analysis is performed. Indeed, the deformation should not introduce any linear and angular displacements. We thus compute the linear and angular displacements induced by the imposed deformation, and subtract them to obtain the final admissible deformations. The deformation velocity $\widetilde{\boldsymbol{u}}(\boldsymbol{x},\, t)$ can be easily computed following surface markers in a Lagrangian way, after having performed the procrustes analysis. To recover $\widetilde{\boldsymbol{u}}(\boldsymbol{x},\, t)$ in Ω_s, interpolation is performed from body mesh values at the boundary Γ_s.

As already mentioned, the linear and angular motions of the i^{th} swimmer are obtained from the Newton's law

$$m_i \frac{\mathrm{d}\overline{\boldsymbol{u}_i}}{\mathrm{d}t} = \boldsymbol{F}_i, \tag{12}$$

$$\frac{\mathrm{d}J_i\boldsymbol{\omega}_i}{\mathrm{d}t} = \boldsymbol{T}_i, \tag{13}$$

where m_i and J_i are the mass and inertia matrix of the i^{th} swimmer, $\boldsymbol{F}_i$ and $\boldsymbol{T}_i$ are the external forces and torques applied on the i^{ith} body surface, and $\overline{\boldsymbol{u}}_i$ and $\boldsymbol{\omega}_i$ denote the linear and angular velocities.

In the absence of contact and collision, when the body in not in a close vicinity of another one, the external forces and the torques are limited to hydrodynamic effects, $\boldsymbol{F}_i = \boldsymbol{F}_i^{\mathtt{hyd}}$ and $\boldsymbol{T}_i = \boldsymbol{T}_i^{\mathtt{hyd}}$, and are computed by

$$\boldsymbol{F}_i^{\mathtt{hyd}} = -\int_{\Gamma_S^{(i)}} \mathbb{T}(\boldsymbol{u},\, p)\, \boldsymbol{n}_i \,\mathrm{d}\boldsymbol{x}, \tag{14}$$

$$\boldsymbol{T}_i^{\mathtt{hyd}} = -\int_{\Gamma_S^{(i)}} \boldsymbol{r}_i \wedge \mathbb{T}(\boldsymbol{u},\, p)\, \boldsymbol{n}_i \,\mathrm{d}\boldsymbol{x}, \tag{15}$$

where $\mathbb{T}(\boldsymbol{u},\, p) = -p\boldsymbol{I} + \mu(\nabla\boldsymbol{u} + \nabla\boldsymbol{u}^T)$ is the stress tensor, $\boldsymbol{n}_i$ is the unit outward vector to $\Gamma_S^{(i)}$, and $\boldsymbol{r}_i = \boldsymbol{x} - \boldsymbol{x}_G^{(i)}$ with $\boldsymbol{x}_G^{(i)}$ the center of mass of the i^{th} swimmer.

The (local) rotation velocity is given by $\boldsymbol{u}_i^{\theta} = \boldsymbol{\omega} \wedge \boldsymbol{r}_i$.

2.6 Lubrication and collisions models

The lubrication and collision models are based on the ones recently introduced in [17] and [18]. The contact and collisions on the i^{th} body are modeled with extra forces $\boldsymbol{F}_i^{\mathtt{col}}$ and torques $\boldsymbol{F}_i^{\mathtt{col}}$. The external forces and torques acting on the i^{th} body are thus $\boldsymbol{F}_i = \boldsymbol{F}_i^{\mathtt{hyd}} + \boldsymbol{F}_i^{\mathtt{col}}$ and $\boldsymbol{T}_i = \boldsymbol{T}_i^{\mathtt{hyd}} + \boldsymbol{T}_i^{\mathtt{col}}$.

2.6.1 Lubrication model

The lubrication model is introduced to correct the hydrodynamic forces $\boldsymbol{F}_i^{\mathtt{hyd}}$ and torques $\boldsymbol{T}_i^{\mathtt{hyd}}$ when the body is close to an other interface. In this case, not enough grid points are usually available in the gap between the two bodies, leading to inaccurate force and torque computations. Mesh refinement can push back this problem, but sooner or later we will still have to deal with it. We can make use of the Local

Lubrication Correction model (LLCM) introduced in [17, 18]. This model writes

$$\boldsymbol{F}_i^{\texttt{hyd}} = -\int_{\Gamma_S^{(i)}} \mathbb{T}(\boldsymbol{u},\, p)\, \boldsymbol{n}_i \,\mathrm{d}\boldsymbol{x} + \boldsymbol{F}_i^{\texttt{lub}}, \tag{16}$$

$$\boldsymbol{T}_i^{\texttt{hyd}} = -\int_{\Gamma_S^{(i)}} \boldsymbol{r}_i \wedge \mathbb{T}(\boldsymbol{u},\, p)\, \boldsymbol{n}_i \,\mathrm{d}\boldsymbol{x} + \boldsymbol{T}_i^{\texttt{lub}}, \tag{17}$$

where $\boldsymbol{F}_i^{\texttt{lub}}$ and $\boldsymbol{T}_i^{\texttt{lub}}$ are the local lubrication force and torque exerted on the i^{th} body.

If a collision model is used, the lubrication forces and torques are negligible with respect to the collision ones, and we thus do not take them into account in what follows.

2.6.2 Collision model

The collision model used in this work is based on the soft-sphere approach introduced in [29, 30]. This collision model, later on used in [18], is accurate, at the price of a large increase of CPU costs. In this paper we use a simplified and faster local collision model to compute $\boldsymbol{F}_i^{\texttt{col}}$ and $\boldsymbol{T}_i^{\texttt{col}}$.

We introduce a collision tensor $\mathbb{T}^{col}$. The computation of forces and torque are thus

$$\boldsymbol{F}_i = -\int_{\Gamma_S^{(i)}} \left(\mathbb{T}(\boldsymbol{u},\, p) + \mathbb{T}^{col}\right) \boldsymbol{n}_i \,\mathrm{d}\boldsymbol{x}, \tag{18}$$

$$\boldsymbol{T}_i = -\int_{\Gamma_S^{(i)}} \boldsymbol{r}_i \wedge \left(\mathbb{T}(\boldsymbol{u},\, p) + \mathbb{T}^{col}\right) \boldsymbol{n}_i \,\mathrm{d}\boldsymbol{x}. \tag{19}$$

The tensor is $\mathbb{T}^{col} = \sum_{k=0}^{N_S} \mathbb{T}_k^{col}$ where the indice $k = 0$ is for the enclosure body.

For any given point $\boldsymbol{x}$ in the computational fluid domain, the collision tensor corresponding to the k^{th} body writes

$$\mathbb{T}_k^{col} = \beta \left((\boldsymbol{u}(\overline{\boldsymbol{x}}_k) - \boldsymbol{u}(\boldsymbol{x})) \otimes \frac{(\overline{\boldsymbol{x}}_k - \boldsymbol{x})}{\|\overline{\boldsymbol{x}}_k - \boldsymbol{x}\|^2} \right) \left(1 - \frac{1}{2}\tanh\left(\frac{2\|\overline{\boldsymbol{x}}_k - \boldsymbol{x}\| - \varepsilon}{12\varepsilon} \right) \right), \tag{20}$$

where $\otimes$ denotes the tensor product and $\overline{\boldsymbol{x}}_k = \arg\min_{\boldsymbol{y}\in\Gamma_S^{(k)}} \|\boldsymbol{x} - \boldsymbol{y}\|$. If the distance $\|\overline{\boldsymbol{x}}_k - \boldsymbol{x}\|$ is quite small, the quantity $\frac{(\overline{\boldsymbol{x}}_k - \boldsymbol{x})}{\|\overline{\boldsymbol{x}}_k - \boldsymbol{x}\|}$ can be approximated using the level set function $-\frac{\nabla\psi_S^{(k)}}{\|\nabla\psi_S^{(k)}\|}$. The parameter β has to be tuned to reach a desired collision force, and we impose $\beta = 1$ in this study. The later term $\left(1 - \frac{1}{2}\tanh\left(\frac{2\|\overline{\boldsymbol{x}}_k - \boldsymbol{x}\| - \varepsilon}{12\varepsilon}\right)\right)$ is an activation term that is almost equal to zero for $\|\overline{\boldsymbol{x}}_k - \boldsymbol{x}\| > \varepsilon$, almost equal to one for $\|\overline{\boldsymbol{x}}_k - \boldsymbol{x}\| < 0$ and varies continuously between these values.

2.7 Numerical methods

The Navier-Stokes equations are discretized on a uniform Cartesian meshes with finite differences. We use second order discretization for all terms expect an upwind third order scheme for the convective terms. The discretization in time follows the fractional step method introduced in [31] and [32].

More details can be found in our previous papers [2, 26, 3, 4].

3 Numerical results

3.1 Simulation parameters

The size of the computational domain Ω is $L_X = L_Z = 40\,cm$ and $L_Y = 6\,cm$. The uniform Cartesian mesh is $N_X \times N_Y \times N_Z = 401 \times 61 \times 401$, *i.e.* approximatively 10 millions of nodes. The uniform discretization step is $h = 1\,mm$. The time step is obtained from a classsical CFL conditions with $CFL = 0.45$, *i.e.* $\Delta t = CFL \frac{h}{max(|u|,|v|,|w|)}$. Numerical simulations are performed over the temporal horizon $t \in [0,\, 120]\, s$.

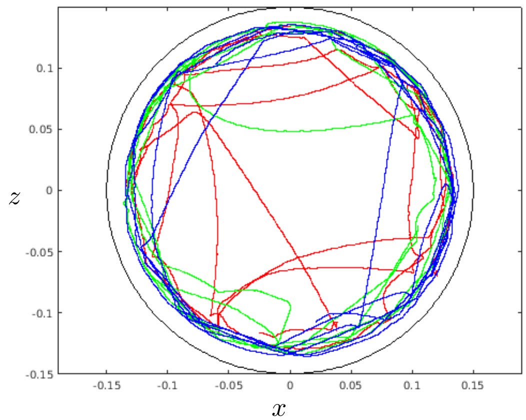

(a) Porous enclosure

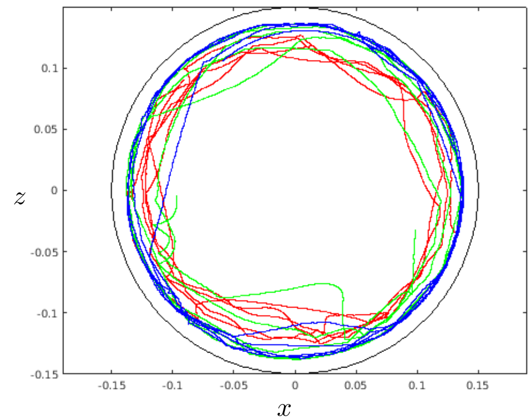

(b) Impermeable enclosure

Figure 4: Temporal evolution of the three-fish group trajectories for $0 \leq t \leq 120\,s$ for porous and impermeable enclosures. Each color represents one fish. Black lines represent the enclosure.

The circular enclosure has a diameter $D = 30\,cm$, with width equal to $1\,cm$ and height equal to $L_Y - \delta_{bottom} - \delta_{top}$. Here we chose $\delta_{top} = 0$, and $\delta_{bottom} = 2h$.

In what follows, we consider a group of three swimming fishes. The length of the fishes is $7.6\,cm$, and the associated wavelength is $\lambda = \ell$. The fishes swim with random frequency $f = \omega/2\pi$ in the range $[3.5, 4.5]\,Hz$ following the swimming law (10).

The activation zone ε for the collision is $\varepsilon = 2h$.

The external boundary conditions on Γ^{ext} are the following:

- periodic boundary conditions are used for both velocity and pressure (for Poisson equation) on lateral boundaries (left-right and front-back from Figure 1(c)).

- Non-slip boundary condition is imposed on the bottom wall, *i.e.* $\boldsymbol{u} = \boldsymbol{0}$, and slip boundary conditions are imposed on the top boundary, *i.e.* $\frac{\partial u}{\partial y} = \frac{\partial w}{\partial y} = 0$ and $v = 0$, homogenous Neumann boundary conditions are used for the Pressure on top and bottom boundaries, *i.e.* $\frac{\partial p}{\partial y} = 0$.

The fluid under consideration is water, with dynamic viscosity $\mu = 0.001\,Pa/s$ and density $\rho = 1000\,kg/m^3$. The density of the swimmers is $\rho_s = 1000\,kg/m^3$.

3.2 Results

We present here preliminary results obtained for a small group of fishes, limited to three swimmers. This is sufficient to observe different kind of contacts, for instance fishes-enclosure and fish-fish.

The temporal evolution of the three-fish group trajectories for $0 \leq t \leq 120\,s$ for porous and impermeable enclosures are presented in Figure 4. While fishes tend to stay near the enclosure for the impermeable case, their motions seem to be more irregular for the porous case.

Snapshots of the fish position with the Q-criterion representation of the flow are plotted in figures 5 and 6 for the impermeable and porous enclosures. It can be seen in figure 6 that a flow is created outside the porous enclosure. In each figure, a focus is given over one collision between two fishes. For the impermeable case, the fishes are easily bypassed, without really taking off from the enclosure. For the porous case, one of the two fish leaves the enclosure. Finally, classical $V-$shaped wakes generated by the fishes are visible in figures 5 and 6 .

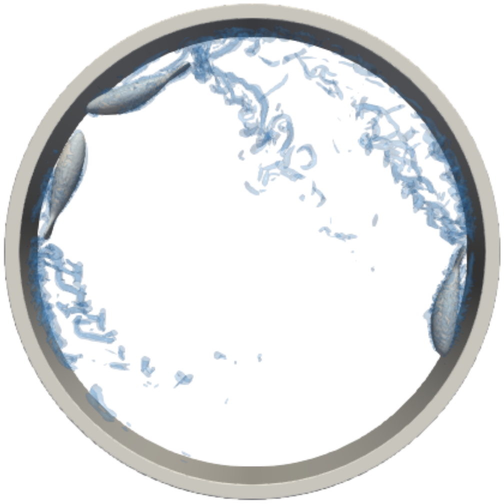

(a) $t = 16\,s$

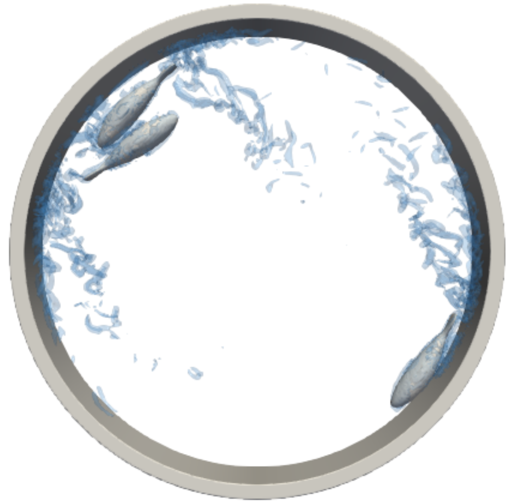

(b) $t = 17\,s$

(c) $t = 18\,s$

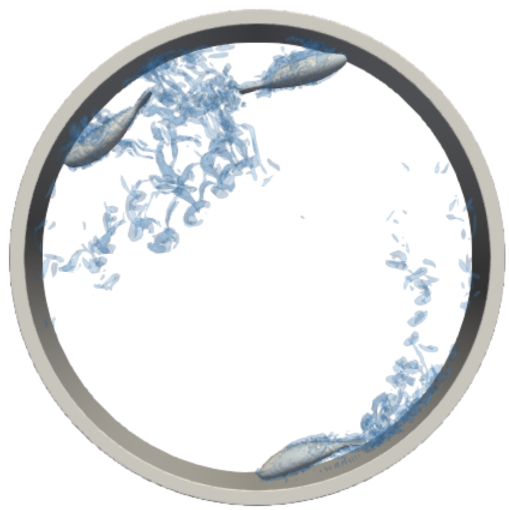

(d) $t = 19\,s$

(c) $t = 20\,s$

(d) $t = 21\,s$

Figure 5: Snapshots for the impermeable enclosure. Q-criterion representation of the flow.

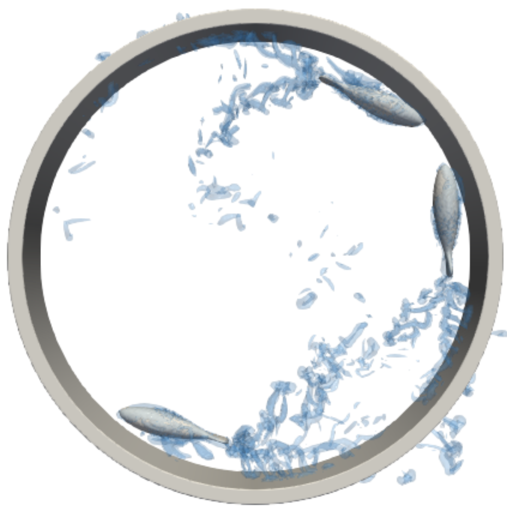

(a) $t = 10\,s$

(b) $t = 11\,s$

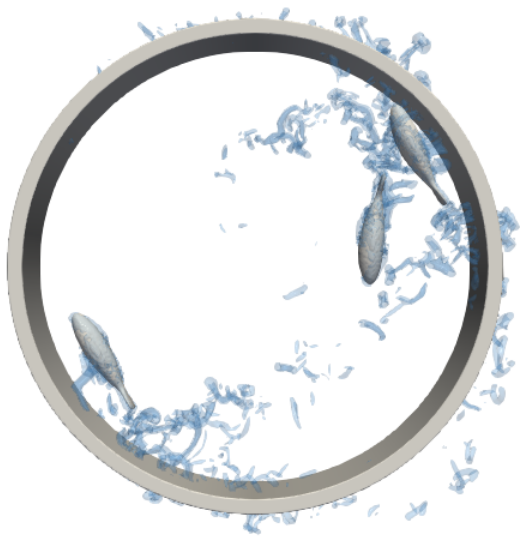

(c) $t = 12\,s$

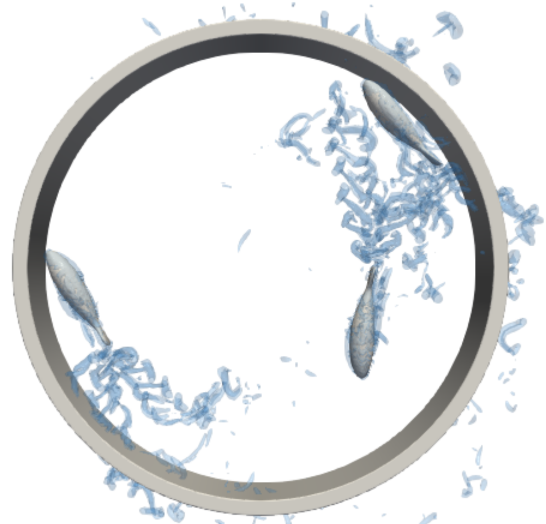

(d) $t = 13\,s$

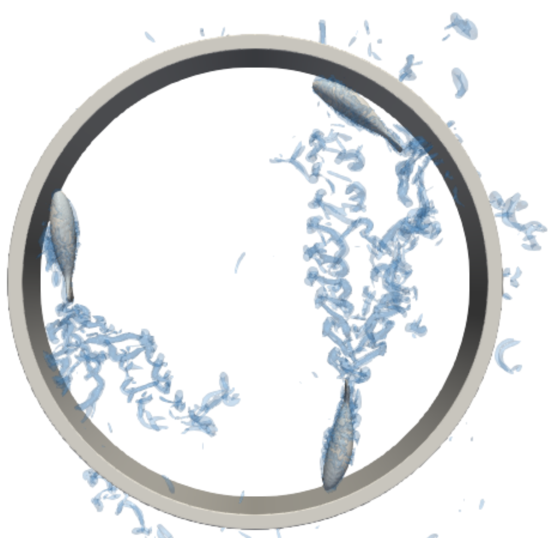

(c) $t = 14\,s$

(d) $t = 15\,s$

Figure 6: Snapshots for the porous enclosure. Q-criterion representation of the flow.

4 Conclusion and Future Work

We have developed a numerical framework to simulate fluid-structure interaction with collisions. While the fluid is classically modeled using the incompressible Navier-Stokes equations, the bodies are taken into account using the Volume Penalization method allowing to use a fixed Cartesian mesh. Simple and robust numerical schemes can thus be used, with a special care at the interface. The collisions are modeled with a collision tensor that is taken into account for the computation of the forces and the torques exerted on the body. This tensor only depends on local geometric and kinematic quantities. Several parameters have however to be tuned. The next step is to automatically calibrate these parameters on some experiments. Finally, we will study in details the influence of the porosity of the enclosure on the swimming behavior for several fish school sizes.

References

[1] A. von Loebbecke, R. Mittal, F. Fish, and R. Mark. Propulsive efficiency of the underwater dolphin kick in humans. *J Biomech Eng.*, 131(5):054504, 2009.

[2] M. Bergmann and A. Iollo. Modeling and simulation of fish-like swimming. *Journal of Computational Physics*, 230(2):329 – 348, 2011.

[3] M Bergmann, A Iollo, and R Mittal. Effect of caudal fin flexibility on the propulsive efficiency of a fish-like swimmer. *Bioinspiration & Biomimetics*, 9(4):046001, 2014.

[4] Michel Bergmann and Angelo Iollo. Bioinspired swimming simulations. *Journal of Computational Physics*, 323:310 – 321, 2016.

[5] D.S. Barrett, M.S. Triantafyllou, D.K.P. Yue, M.A. Grosenbauch, and M.J. Wolfgang. Drag reduction in fish-like locomotion. *J. Fluid Mech.*, 392:182–212, 1999.

[6] M.S. Triantafyllou, G.S. Triantafyllou, and D.K.P Yue. Hydrodynamics of fishlike swimming. *Annual Review of Fluid Mechanics*, 32, 2000.

[7] Q. Zhu, M.J. Wolfgang, D.K.P. Yue, and M.S. Triantafyllou. Three-dimensional flow structures and vorticity control in fish-like swimming. *J. Fluid Mech.*, 468:1–28, 2002.

[8] George Lauder, Peter Madden, Ian Hunter, James Tangorra, Naomi Davidson, Laura Proctor, Rajat Mittal, Haibo Dong, and Meliha Bozkurttas. Design and performance of a fish fin-like propulsor for auvs. 01 2005.

[9] Meliha Bozkurttas, James Tangorra, George Lauder, and Rajat Mittal. Understanding the hydrodynamics of swimming: From fish fins to flexible propulsors for autonomous underwater vehicles. In *Mining Smartness from Nature (CIMTEC 2008)*, volume 58 of *Advances in Science and Technology*, pages 193–202. Trans Tech Publications Ltd, 2 2009.

[10] D.H. Cushing and F.R. Harden-Jones. Why do fish school? *Nature*, 218:918–920, 1968.

[11] W. Weihs. Hydrodynamics of fish schooling. *Nature*, 241:290–291, 1973.

[12] Gen Li, Dmitry Kolomenskiy, Hao Liu, Benjamin Thiria, and Ramiro Godoy-Diana. Hydrodynamical fingerprint of a neighbour in a fish lateral line. *Frontiers in Robotics and AI*, 9, 2022.

[13] Julian A. Simeonov and Joseph Calantoni. Modeling mechanical contact and lubrication in direct numerical simulations of colliding particles. *International Journal of Multiphase Flow*, 46:38–53, 2012.

[14] A. Lefebvre-Lepot, B. Merlet, and T. N. Nguyen. An accurate method to include lubrication forces in numerical simulations of dense stokesian suspensions. *Journal of Fluid Mechanics*, 769:369–386, 2015.

[15] Y NGUYEN, John WELLS, and Hung TRUONG. Fictitious-domain simulation of solid-liquid flow with subgrid lubrication force correction; a sphere falling onto a plane surface. *PROCEEDINGS OF HYDRAULIC ENGINEERING*, 51:151–156, 2007.

[16] Pedro Costa, Bendiks Jan Boersma, Jerry Westerweel, and Wim-Paul Breugem. Collision model for fully resolved simulations of flows laden with finite-size particles. *Phys. Rev. E*, 92:053012, Nov 2015.

[17] B. Lambert, L. Weynans, and M. Bergmann. Local lubrication model for spherical particles within incompressible navier-stokes flows. *Phys. Rev. E*, 97:033313, Mar 2018.

[18] B. Lambert, L. Weynans, and M. Bergmann. Methodology for Numerical Simulations of Ellipsoidal Particle-Laden Flows. *International Journal for Numerical Methods in Fluids*, 2020.

[19] S. Osher and J. A. Sethian. Fronts propagating with curvature-dependent speed: Algorithms based on hamilton-jacobi formulations. *J. Comput. Phys.*, 79(12), 1988.

[20] J. A. Sethian. *Level Set Methods and Fast Marching Methods*. Cambridge University Press, Cambridge, UK, 1999.

[21] C.S. Peskin. Flow patterns around heart valves: A numerical method. *J. Comp. Phys.*, 10:252–275, 1972.

[22] R. Mittal and G. Iaccarino. Immersed boundary methods. *Annu. Rev. Fluid Mech.*, 37:239–261, 2005.

[23] R. Mittal, H. Dong, M. Bozkurttas, F.M. Najjar, A. Vargas, and A. von Loebbecke. A versatile sharp interface immersed boundary method for incompressible flows with complex boundaries. *Journal of Computational Physics*, 227(10):4825 – 4852, 2008.

[24] Anup A. Shirgaonkar, Malcolm A. MacIver, and Neelesh A. Patankar. A new mathematical formulation and fast algorithm for fully resolved simulation of self-propulsion. *Journal of Computational Physics*, 228(7):2366 – 2390, 2009.

[25] P. Angot, C.H. Bruneau, and P. Fabrie. A penalization method to take into account obstacles in a incompressible flow. *Num. Math.*, 81(4):497–520, 1999.

[26] M. Bergmann, J. Hovnanian, and A. Iollo. An accurate cartesian method for incompressible flows with moving boundaries. *Communications in Computational Physics*, 15(5):1266–1290, 2014.

[27] Alexander J. Smits. Undulatory and oscillatory swimming. *Journal of Fluid Mechanics*, 874, 2019.

[28] Pan Han, Junshi Wang, Frank Fish, and Haibo Dong. Kinematics and hydrodynamics of a dolphin in forward swimming. 06 2020.

[29] P. Costa, B. J. Boersma, J. Westerweel, and W. P. Breugem. Collision model for fully-resolved simulations of flows laden with finite-size particles. *Physical Review E*, 92(5), 10/2015.

[30] J. C. Brändle de Motta, W. P. Breugem, B. Gazanion, J. L. Estivalezes, S. Vincent, and E. Climent. Numerical modelling of finite-size particle collisions in a viscous fluid. *Physics of Fluids*, 25:083302, 2013.

[31] A.J. Chorin. Numerical solution of the Navier-Stokes equations. *Math. Comp.*, 22:745–762, 1968.

[32] R. Temam. Sur l'approximation de la solution des equations de navier-stokes par la methode des pas fractionnaires ii. *Archiv. Rat. Mech. Anal.*, 32:377–385, 1969.